ARTICLE

BIOTECHNOLOGY and BIOENGINEERING

384 Hanging Drop Arrays Give Excellent *Z*-Factors and Allow Versatile Formation of Co-Culture Spheroids

Amy Y. Hsiao,[1] Yi-Chung Tung,[1,2] Xianggui Qu,[3] Lalit R. Patel,[1,4] Kenneth J. Pienta,[4,5] Shuichi Takayama[1,6,7]

[1]Department of Biomedical Engineering, University of Michigan, 2215 Carl A Gerstacker Bldg, 2200 Bonisteel Blvd, Ann Arbor, Michigan 48109; telephone: +1-734-615-5539; fax: +1-734-936-1905; e-mail: takayama@umich.edu

[2]Research Center for Applied Sciences, Academia Sinica, Taipei, Taiwan

[3]Department of Mathematics and Statistics, Oakland University, Rochester, Michigan

[4]Department of Internal Medicine, University of Michigan Medical School, Ann Arbor, Michigan

[5]Department of Urology, University of Michigan Medical School, Ann Arbor, Michigan

[6]Macro Molecular Science and Engineering, University of Michigan, Ann Arbor, Michigan

[7]School of Nano-Biotechnology and Chemical Engineering WCU Project, UNIST, Ulsan, Republic of Korea

Received 22 September 2011; revision received 21 November 2011; accepted 23 November 2011

Published online 7 December 2011 in Wiley Online Library (wileyonlinelibrary.com). DOI 10.1002/bit.24399

ABSTRACT: We previously reported the development of a simple, user-friendly, and versatile 384 hanging drop array plate for 3D spheroid culture and the importance of utilizing 3D cellular models in anti-cancer drug sensitivity testing. The 384 hanging drop array plate allows for high-throughput capabilities and offers significant improvements over existing 3D spheroid culture methods. To allow for practical 3D cell-based high-throughput screening and enable broader use of the plate, we characterize the robustness of the 384 hanging drop array plate in terms of assay performance and demonstrate the versatility of the plate. We find that the 384 hanging drop array plate performance is robust in fluorescence- and colorimetric-based assays through *Z*-factor calculations. Finally, we demonstrate different plate capabilities and applications, including: spheroid transfer and retrieval for Janus spheroid formation, sequential addition of cells for concentric layer patterning of different cell types, and culture of a wide variety of cell types.

Biotechnol. Bioeng. 2012;109: 1293–1304.

KEYWORDS: spheroid; *Z*-factor; high-throughput; 3D; hanging drop

Correspondence to: S. Takayama

Contract grant sponsor: Coulter Foundation
Contract grant sponsor: College of Engineering Translational Research Fund
Contract grant sponsor: University of Michigan
Contract grant sponsor: NIH
Contract grant number: 1 PO1 CA093900

Introduction

Need for High-Throughput 3D Cell Assays

High-throughput 3D cell culture is motivated by the need to work with accurate in vitro models in drug discovery and therapy test programs. Various cell types have been shown to behave differently when cultured under 2D versus 3D (Yamada and Cukierman, 2007) conditions. Currently, however, most initial studies in drug development are still based on 2D cell assays, which often skew research results and have limited predictive power in clinical efficacy (Hirschhaeuser et al., 2010). Since the time and costs of drug development increase substantially during the animal models phase and even more in the subsequent clinical trials, it is crucial to identify promising candidates accurately in the early developmental stages. Implementation of high-throughput 3D cell culture screening assays is anticipated as a potent tool to expedite and accurately select key molecules in drug development. To promote wider usage of 3D cultures in research and pharmaceutical development, we have successfully developed the 384 hanging drop array plate (Fig. 1a) for high-throughput spheroid culture that offers simplified liquid handling procedures and compatibility with high-throughput screening (HTS) instruments (Tung et al., 2011). Here, we further characterize the quality of HTS assays performed on the 384 hanging drop array plate for practical high-throughput 3D cell culture screening assays.

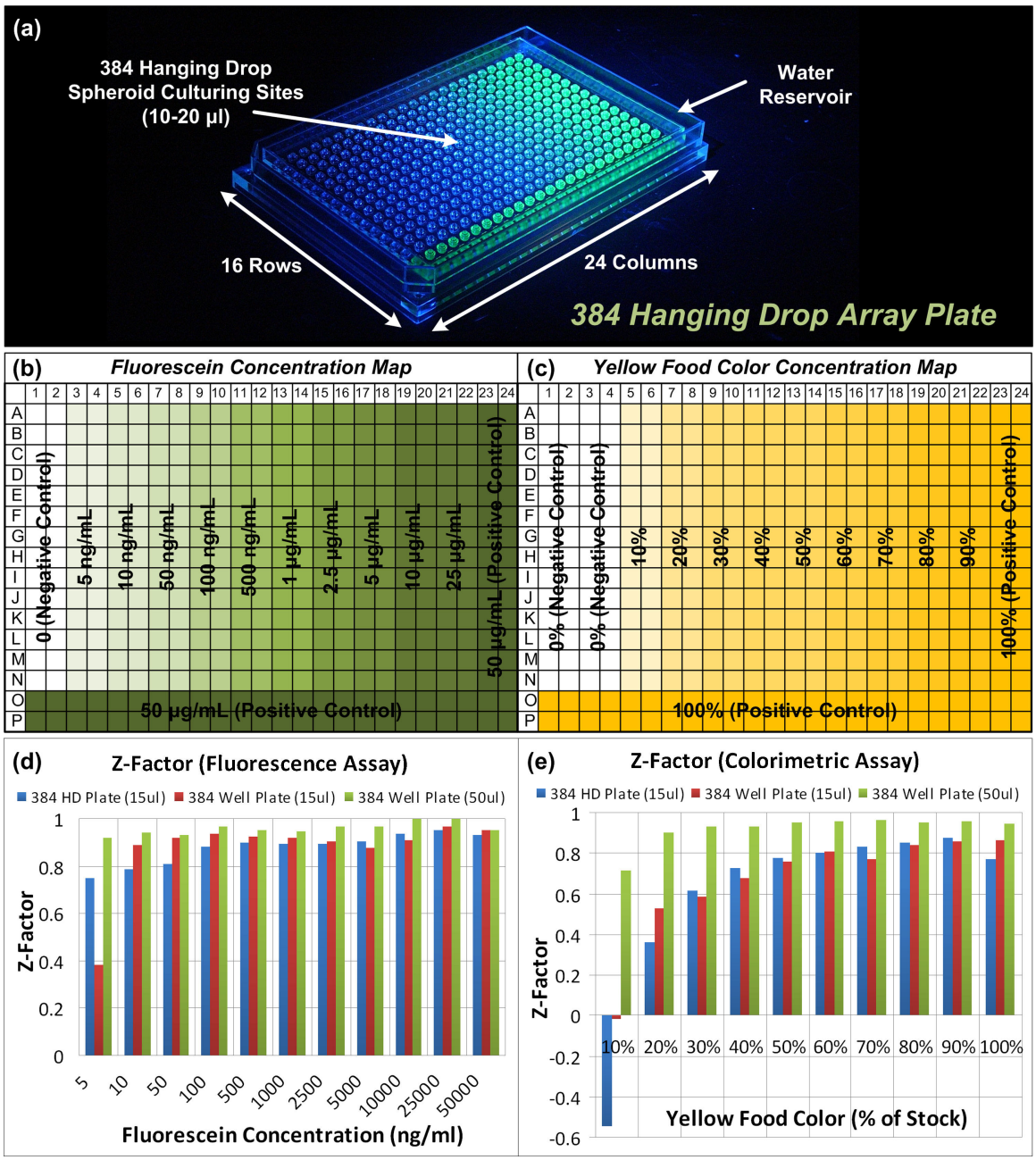

Figure 1. **a**: An actual image of the 384 hanging drop array plate highlighting the key features and specifications. **b**: Concentration map in 384-format plate for fluorescein solution. **c**: Concentration map in 384-format plate for yellow food color solution. **d**: Bar graph showing the summary of *Z*-factors for fluorescence-based assay at various fluorescein concentrations. **e**: Bar graph showing the summary of *Z*-factors for colorimetric-based assay at various percentages of yellow food color. [Color figure can be seen in the online version of this article, available at http://wileyonlinelibrary.com/bit]

Z′- and *Z*-Factor

HTS is an essential initial step in drug discovery. The ability to identify true active compounds ("hits") depends greatly on the quality of assays and proper analysis of data (Sui and Wu, 2007; Zhang et al., 1999). Therefore, high-throughput 3D cell culture needs reliable assays for endpoint analysis to obtain accurate readouts. In most HTS experiments, because each compound is only tested in singlet or duplicate, a high degree of accuracy and sensitivity in the assay is critical for identifying hits (Zhang et al., 1999). A high quality HTS assay must be able to identify the few compounds with desired biological activity with high confidence. Over the past decade, researchers from the HTS community have used the *Z*-factor (Zhang et al., 1999) as a widely accepted standard to evaluate the quality of a HTS assay.

Z′- or Z-factor is an assay performance measurement that provides an easy and useful summary of assay quality and

robustness (Birmingham et al., 2009; Sui and Wu, 2007; Zhang et al., 1999). Z'-factor is typically used in assay optimization as it is based on controls, whereas Z-factor is often used during screening to assess performance of the screen on actual samples (Birmingham et al., 2009; Zhang et al., 1999). Z'- and Z-factors are defined as follows (Zhang et al., 1999):

$$Z'\text{-factor} = 1 - \frac{3s_{hc} + 3s_{lc}}{|\overline{x}_{hc} - \overline{x}_{lc}|}$$

$$Z\text{-factor} = 1 - \frac{3s_{s} + 3s_{c}}{|\overline{x}_{s} - \overline{x}_{c}|}$$

$\overline{x}$ indicates mean, s indicates standard deviation, "hc" indicates the high-value control (positive control), "lc" indicates the low-value control (negative control), "s" indicates sample value, and "c" indicates negative control. The range of both measures is from negative infinity to 1, with >0.5 as a very good assay, >0 an acceptable assay, and <0 an unacceptable assay (Birmingham et al., 2009; Zhang et al., 1999). To characterize the performance of our 384 hanging drop plate for fluorescence- and colorimetric-based assays, we utilized various concentrations of fluorescein and yellow food color liquid as sample drops to calculate the Z'- and Z-factors. For both fluorescence-and colorimetric-based assays, we show that the Z'- and Z-factors calculated for the 384 hanging drop plate are comparable to those values obtained from commercially-available clear 384-well plates.

Techniques and Applications of Spheroid Cultures

Many types of mammalian cells spontaneously aggregate into 3D spheroids when cultured in environments where cell–cell interactions dominate over cell–substrate interactions (Friedrich et al., 2009; Hirschhaeuser et al., 2010; Lin and Chang, 2008). Recent realization of the importance of 3D cell culture has attracted more researchers to adapt 3D spheroid cultures into biological studies. Compared to conventional 2D monolayer cultures, 3D spheroids resemble physiological tissues and tumors much better in terms of structural and functional properties (Lin and Chang, 2008). Various primary or progenitor-like cell types also show significantly enhanced viability and functions when grown as spheroids (Lin and Chang, 2008). Recently, spheroid research has been devoted to various areas in biology including cancer biology, developmental biology, tissue engineering, and other disciplines. Specifically, spheroids serve as excellent models for solid tumors, components in bioartificial livers (Lin and Chang, 2008), cellular building blocks in tissue engineering, and embryoid bodies. Tumor spheroids can be used to study various types of cancers that are found growing as spherical aggregates in vivo, such as the ascites in ovarian cancer (Shields et al., 2009). They have also been used widely as models to study cancer stem cells, cancer metastasis, invasion, and for therapeutic screening (Hirschhaeuser et al., 2010; Lin and Chang, 2008). In addition, spheroids can also be applied to study cellular migration and tumor dissemination from 3D constructs, signaling and crosstalk between cells cultured in 3D environments (secreted autocrine and paracrine factors from 3D constructs with inherent metabolic profiles and diffusion/transport limitations), 3D cell–cell interactions and confrontational studies, differentiation of stem cells from co-cultures of different cell types or addition of factors, and 3D patterning for tissue engineering purposes. However, many of these studies require sophisticated manipulation and analysis techniques not commonly attainable through current spheroid formation platforms, such as formation of uniform pool of spheroids, formation of multi-cell type mixed co-culture spheroids, sequential addition of reagents, and retrieval and addition of single cell suspensions or spheroids. Conventional spheroid formation methods such as culture of cells on non-adhesive surfaces, spinner flasks, and NASA rotary systems have poor uniformity control over spheroid size, lack individual compartment for each sample, and often require specialized equipments (Ingram et al., 1997; Lin and Chang, 2008; Friedrich et al., 2007), thus making HTS and testing of therapeutic compounds on spheroid samples almost impossible. Commercially available microwell-based embryoid bodies production plates allow for mass production of uniformly sized embryoid bodies and spheroids (Baraniak and McDevitt, 2011; Bratt-Leal et al., 2011), but would also require additional compartmentalization to perform HTS applications. Recently developed micro- and nanotechnology based spheroid formation and culture platforms utilizing arrays of microwells, posts, micropatterns, 3D scaffolds, or nanoimprinted scaffolds offer control over spheroid uniformity and introduce individual compartment for each sample (Karp et al., 2007; Kojima et al., 2009; Powers et al., 2002; Tamura et al., 2008; Toh et al., 2009; Torisawa et al., 2007a,b; Ungrin et al., 2008; Yoshii et al., 2011; Zhang et al., 2008). However, many such devices have material compatibility issues with hydrophobic drugs, and spheroid samples are often difficult to retrieve from these sophisticated microdevices for further analyses. Most importantly, the complexity typically involved in such device fabrication (and sometimes operation) prevents mass production, and greatly hinders the biological community from adapting such technologies more widely. Here, we demonstrate the simplicity and versatility of our HTS compatible plate with biomedical applications in the formation of a wide variety of spheroids from different cell types, concentric layer patterning of different cell types into spheroids, mixed co-culture spheroid formation, and spheroid transfer for 3D cell confrontations.

Materials and Methods

Design and Fabrication of the 384 Hanging Drop Array Plate

384 hanging drop array plates are fabricated by injection molding with the plate specifications described previously (Tung et al., 2011).

Z′- and *Z*-Factor Calculations

To calculate the *Z′*- and *Z*-factor of the 384 hanging drop array plate for fluorescence- and colorimetric-based assays, we formed 15 μL hanging drops in all 384 sites of the plate from various concentrations of fluorescein (sodium salt, F6377, Sigma–Aldrich Corp., St. Louis, MO) and yellow food color (McCormick & Company, Inc., Sparks, MD), respectively, according to the concentration maps shown in Figure 1b,c. This type of one column and one row control placement is a method to guard against and to overcome positional effects in HTS (Qu, 2011). Such control placement setups are designed so that one would be able to normalize the plate reader results if there were any positional effects (Qu, 2011). By keeping the contents of all the wells in a single column and a single row constant, it would be possible to take out the positional effects contributing from each column and row and thus normalize the entire plate.

For fluorescence-based assay, 1 mg/mL stock solution of fluorescein was first prepared and dissolved in phosphate-buffered saline (PBS; Gibco 10010, Invitrogen Co., Carlsbad, CA). The stock solution was subsequently serially diluted to all the concentrations listed in the map (Fig. 1b, range from PBS only—negative control to 50 μg/mL—positive control). 384 15 μL hanging drops were then manually formed in the 384 hanging drop plate from all the concentrations of fluorescein solutions using a multi-channel pipettor. The plate was then read on a microplate reader (PHERAStar FS, BMG Labtech, Ortenberg, Germany) from the bottom of the plate, with 485 nm excitation and 520 nm emission, to obtain fluorescence intensity readouts. *Z′*- and *Z*-factors at each fluorescein concentration were then calculated from the fluorescence intensity readings according to the formulas mentioned in the *Z′*- and *Z*-Factor Section.

For colorimetric-based assay, 100% solution of yellow food color was first prepared by adding 175 μL of stock yellow food color into 100 mL of distilled water (Gibco 15230, Invitrogen Co.). A percentage dilution, beginning with the 100% solution of yellow food color, was then performed to make all the percentages listed in the map (Fig. 1c, range from distilled water only—negative control to 100% yellow food color solution—positive control). 384 15 μL hanging drops were then manually formed in the 384 hanging drop plate from all the percentages of yellow food color solutions using a multi-channel pipettor. The plate was then read on a microplate reader (PHERAStar FS, BMG Labtech) to determine the absorbance of each yellow food color percentage at 405 nm. *Z′*- and *Z*-factors at each yellow food color percentage were then calculated from the absorbance readouts according to the formulas mentioned in the *Z′*- and *Z*-Factor Section.

The same fluorescein and yellow food color solutions were also pipetted into standard, clear, polystyrene 384-well plates (Corning COSTAR 3701) at two volumes (15 and 50 μL) using a robotic liquid handler (CyBi-Well, CyBio, Inc., Jena, Germany) in the same concentration pattern as the 384 hanging drop plates (Fig. 1b,c). The plates were subsequently read on a microplate reader (PHERAStar FS, BMG Labtech) using the same settings as for the 384 hanging drop plates to obtain fluorescence intensity and absorbance readouts. *Z′*- and *Z*-factors at each yellow food color percentage were then calculated from the fluorescence intensity and absorbance readouts according to the formulas mentioned in the *Z′*- and *Z*-Factor Section for comparison with the data from the 384 hanging drop plates.

General Cell Culture

Murine embryonic stem (mES) cells (ES-D3 cell line; ATCC, Manassas, VA) were cultured in dishes coated with 0.1% w/v porcine gel (Sigma–Aldrich Co.) and maintained in complete medium consisting of Dulbecco's modified Eagle's medium (DMEM) (Gibco 11960, Invitrogen Co.) with 15% v/v fetal bovine serum (FBS) (Gibco 10082, Invitrogen Co.), 4 mM L-glutamin (Invitrogen Co.), 0.1 mM 2-mercapto-ethanol (Sigma–Aldrich Co.), 0.02% v/v sodium pyruvate (Sigma–Aldrich Co.), 100 U/mL penicillin (Invitrogen Co.), 100 U/mL streptomycin (Invitrogen Co.), and 1000 U/mL ESGRO (Invitrgoen Co.) which contains leukemia inhibitory factor (LIF). When D3 mES cells were formed into embryoid bodies, the cells were cultured in complete medium without LIF. D3 mES cells were stably transfected with OCT4-EGFP plasmid construct as previously described (Torisawa et al., 2009), and denoted as mES-Oct4-GFP cells. HepG2 hepatocellular carcinoma cell line (ATCC) and COS7 African green monkey kidney fibroblast cell line (ATCC) were cultured in DMEM (Gibco 11965, Invitrogen Co.) with 10% v/v FBS (Gibco 10082, Invitrogen Co.), and 1% v/v antibiotic–antimicotic (Gibco 15240, Invitrogen Co.). COS7 cells were stained with CellTracker Red CMTPX (1.5 μM, Invitrogen Co.) or CellTracker Green CMFDA (1.5 μM, Invitrogen Co.) for 1 h before seeding the cells into hanging drops. DU145 (ATCC) and PC-3 (ATCC) prostate cancer cell lines were cultured in RPMI-1640 (Gibco 61870, Invitrogen Co.) with 10% v/v FBS (Gibco 10082, Invitrogen Co.), and 1% v/v antibiotic-antimicotic (Gibco 15240, Invitrogen Co.). $DU145^{Luc}$ cells were constructed by stably transfecting DU145 cells with luciferase expressing pLazarus retroviral construct using methods described previously (Kalikin et al., 2003). $PC\text{-}3^{DsRed}$ cells that stably express the DsRed protein were transfected via DsRed lentivirus as previously described (Hsiao et al., 2009). HFOB human fetal osteoblasts (ATCC) were cultured in D-MEM/F-12 (Gibco 10565, Invitrogen Co.) with 10% v/v FBS (Gibco 10082, Invitrogen Co.), and 1% v/v antibiotic–antimicotic (Gibco 15240, Invitrogen Co.). MC3T3-E1 murine pre-osteoblasts (ATCC) were cultured in α-MEM (Alpha Minimum Essential Medium; Gibco A10490, Invitrogen Co.) supplemented with 15% (v/v) FBS (Gibco 10082, Invitrogen Co.), and 1% v/v antibiotic-antimicotic (Gibco 15240, Invitrogen Co.). Differentiation of MC3T3-E1 cells into osteoblasts was

only induced when cultured as spheroids by addition of 50 μg/ml ascorbic acid (Sigma–Aldrich Co.). HUVEC human umbilical vein endothelial cells (Lonza, Basel, Switzerland) passage number 2–6 were cultured in endothelial growth medium-2 (EGM-2, Lonza). When different cell types were co-cultured together, the cells were cultured in media containing fractions of each cell type's growth media at the co-culture ratios. All the cells were cultured in a humidified incubator (37°C in an atmosphere of 5% CO_2). Cell suspensions for the hanging drop experiments were made by dissociating cells with 0.25% trypsin–EDTA (Gibco 25200, Invitrogen Co.), followed by centrifugation of the dissociated cells at 1,000 rpm for 5 min at room temperature, and re-suspended in the appropriate growth media. Cell density was estimated using a hemocytometer.

Spheroid Formation, Co-Culture Spheroid Formation, Concentric Layer Patterning, and Spheroid Transfer in the 384 Hanging Drop Array Plate

General monoculture spheroid formation was performed as previously described (Tung et al., 2011). Briefly, 15 μL of desired cell suspension was pipetted into an access hole in the 384 hanging drop array plate directly from the top, with the pipette tip extending just slightly below the bottom plate surface during the release of the cell suspension. Due to hydrophilicity of the plate and surface tension of the liquid, a cell suspension droplet would hang from the bottom surface of the plate with a meniscus forming in the opening neck region of the access hole. Mixed co-culture spheroids were generated by first preparing mixed cell suspensions from the desired cell types at the specified ratios followed by the same hanging drop formation protocol for monoculture spheroids. Concentric layer patterning of different cell types (or the same cell type labeled with different colors) within a spheroid was achieved by initially forming a monoculture spheroid of one cell type as the inner core. After one day, or once the initial cell type aggregates, 5 μL single cell suspension of the second cell type was subsequently added to the existing hanging drop to form an exterior coating around the inner core. Spheroid transfer within the hanging drop plate for Janus spheroid (Torisawa et al., 2009) formation or 3D cellular confrontation was achieved by direct pipetting to retrieve spheroid from the top of an access hole and then gently pipette into another existing hanging drop containing spheroid just like the removal and addition of liquid (Fig. 5a). Such spheroid transferring process was demonstrated by both manual pipetting and a liquid handling robot (CyBi-Well, CyBio, Inc.).

Spheroid Monitoring and Viability Staining

Spheroids that formed in the hanging drops were routinely imaged by phase contrast microscopy as well as fluorescence microscopy (when applicable) (Nikon TE-300). Individual spheroids were each monitored for 6 to 13 days. On the last day of culture for HepG2, $DU145^{Luc}$, and HFOB spheroids, the spheroids were stained with LIVE/DEAD Viability/Cytotoxicity Kit for mammalian cells (L3224, Invitrogen Co.) to evaluate cellular viability. Five microliters of Calcein AM (8 μM) and Ethidium homodimer-1 (EthD-1, 16 μM) working solution diluted in PBS was directly pipetted into the existing 15 μL hanging drops containing the spheroid samples to achieve a final concentration of 2 μM Calcein AM and 4 μM EthD-1. The samples were subsequently incubated for 30 min at 37°C. After incubation, the stained spheroid samples in the hanging drops were imaged by fluorescence microscopy (Nikon TE-300). The LIVE/DEAD kit determines cell viability based on cell membrane integrity. Live cells are stained by Calcein AM, which emit green fluorescence (517 nm) when excited by blue light (494 nm); whereas dead cells are stained by EthD-1, which emit red fluorescence (617 nm) when excited by green light (528 nm).

Results and Discussion

Z′- and *Z*-Factor of the 384 Hanging Drop Array Plate

Since one of the most important applications of the 384 hanging drop plate is HTS for novel drugs, it is important to know the quality of various assays performed in the hanging drop plate. We adapted the calculation of Z′- and *Z*-factors as assay performance measures to validate the robustness of fluorescence- and colorimetric-based assays in the 384 hanging drop plate. Figure 1d,e summarizes the Z′- and *Z*-factor calculations and comparisons for both the 384 hanging drop plate and the standard clear 384-well plate.

For fluorescence-based assays, *Z*-factors are all well-above 0.5 at all the fluorescein concentrations tested in the 384 hanging drop plate. This indicates that the fluorescence-based assays performed in the 384 hanging drop plate are excellent within the range of concentrations tested. In addition, the *Z*-factors for the 384 hanging drop plate are all comparable to the *Z*-factors for the commercially available, standard, clear 384-well plate. The *Z*-factors are anticipated to be even better if the 384 hanging drop plates are made of solid black polystyrene with solid walls around each hanging drop access hole to segregate each drop. Typical fluorescence-based assays are performed in solid black polystyrene multi-well plates as the black walls can reduce well-to-well crosstalk and background for fluorescent assay. Nevertheless, the ability to conduct microscopy imaging would be compromised if the 384-well plates are made of solid black material. Various design considerations and complications must be carefully reviewed before making such a step.

For colorimetric-based assays, with the exception of the lowest two yellow food color percentages, all the other percentages have *Z*-factors above 0.5 in the 384 hanging drop plate. This indicates that the colorimetric-based assays

performed in the 384 hanging drop plate are excellent within the 30–100% yellow food color solutions tested. It is interesting to note that the 384-well plate (50 μL) appears to consistently outperform the other two plates with higher *Z*-factors at all the percentages tested. This trend is expected since the 50 μL 384-well plate in general has the largest absorbance compared to the other two plates. The absorbance values are proportional to the thickness of the sample (and thus the yellow food color volume in each well, given the same type of plate). The greater the volume, the "thicker" the sample, and the larger the absorbance should be. With higher overall sample mean values in the 50 μL plate, the *Z*-factors also become better. In addition, colorimetric assay values depend on the path of liquid through which light passes. The hanging drops may have a disadvantage due to droplet shape and complex plate shape that light must pass through compared to conventional plates which have relatively flat meniscus and flat plastic, whereas we have rounded meniscus on top and bottom and a complex geometry of the plate. With such complex shapes of plate and droplets, light going through may scatter and diffract more, leading to larger variations between samples. Moreover, the fact that the hanging drops were formed by using a multi-channel pipettor to manually pipette into the hanging drop plate (instead of using a 96-head liquid handling robot to pipette into the 15 and 50 μL 384-well plates) subjected the hanging drop plate to slightly larger variation in the final drop volumes. This higher sample standard deviation contributes to lower *Z*-factors. Finally, the plate reader might not be sensitive enough to read the absorbance at 10% and 20% yellow food color. As a result, a huge variation is generated in these low-value readouts, leading to low and even negative *Z*-factors. Caution must be used when performing colorimetric-assays in the plates involving such low absorbance values. Nevertheless, the *Z*-factors for the 384 hanging drop plate are still comparable to the *Z*-factors for the standard, clear 384-well plate at most yellow food color percentages tested.

It should also be noted that because the detection sensitivity, amount of cross-talk, and positional effects reflected in the plate reader readouts greatly depend on the make and model of the microplate readers, the calculated *Z*′- and *Z*-factors will also change depending on the specific microplate reader used. One should be consistent (and careful in choosing) in plate reader usage throughout the entire experiment from the initial evaluation of the robustness of the assays (*Z*′- and *Z*-factor calculations) to performing the actual assays in HTS.

Biomedical Applications of the 384 Hanging Drop Array Plate

To allow more researchers to adapt the 384 hanging drop array plate for 3D spheroid culture, the platform must be versatile and applicable to a wide variety of studies. Here, we demonstrate several useful techniques made possible by the 384 hanging drop plate that would otherwise be difficult to perform utilizing other spheroid formation and culturing methods. We first demonstrate that 384 hanging drop array plate can be used to generate uniform monoculture spheroids at various defined sizes from mouse embryonic stem cells (mES-Oct4-GFP) (Fig. 2a), HepG2 cells (Fig. 2b), $DU145^{Luc}$ prostate cancer cells (Fig. 3a), and HFOB human fetal osteoblasts (Fig. 3b). Week-long cultures of these spheroids were possible with reasonable viability of cells confirmed on the last day of culture. It should be noted that with an inherent oxygen gradient within larger spheroid samples, more dead cells are expected at the inner core of spheroids. Uniform pool of spheroids and spheroid sizes are controlled by introducing defined numbers of cells to each hanging drop. Such uniformity control feature is often very tedious or not possible in conventional spheroid formation methods. Emerging microtechnologies for spheroid formation (Fukuda et al., 2006; Lee et al., 2010; Sakai and Nakazawa, 2007; Toh et al., 2007; Torisawa et al., 2007a,b; Ungrin et al., 2008; Wu et al., 2008) generally offer considerable improvements for spheroid uniformity control, but such custom-made delicate devices are often tedious to fabricate and require specialized trainings to operate, and thus not readily available to the research community. The 384 hanging drop plate delivers the same advantage in a user-friendly manner.

Next, we show the ability of the hanging drop plate to form mixed co-culture spheroids with randomly-distributed cell types. Figure 4a shows the image of a mixed co-culture spheroid containing $PC\text{-}3^{DsRed}$, HUVEC, and MC3T3-E1 cells at 1:50:50 ratio. Formation of co-culture spheroids using conventional rotating bioreactors and non-adherent surfaces may not ensure uniform incorporation of all co-culture cell types into the spheroids. Many times multiple types of spheroids comprised primarily of just one of the co-culture cell types rather than mixed co-culture spheroids are formed. The hanging drop method overcomes this issue by forcing all cell types to aggregate into a single spheroid by gravity, making formation of mixed co-culture spheroids as simple as monoculture spheroids. Seeding of cells inside sophisticated microwells followed by centrifugation would also promote co-culture cells to settle and aggregate into single clusters, especially inside round-bottom and V-bottom microwells. Nevertheless, the hanging drop system inherently offers the convenience of utilizing natural gravity force to aggregate cells into a single spheroid gently. Without the need of external forces such as centrifugation, the hanging drop system prevents the generation of additional shear forces that may be damaging to more delicate cell types. Moreover, the hanging drop system has the unique advantage of lacking a bottom substrate for cells to eventually attach to over long-term cultures (which are frequently required in various time-extensive co-culture experiments to study heterotypic cell–cell interactions). In addition, concentric layer patterning of multiple cell types (Fig. 4b,c; see the following paragraph) may be difficult to accomplish by centrifugation as it is very likely that cells

would all be settled to the bottom as opposed to gently surrounding the existing spheroids.

We then move on to show that co-culture spheroids can also be patterned in concentric layers. Figure 4b demonstrates a PC-3^{DsRed} and MC3T3-E1 co-culture spheroid at 1:100 ratio with PC-3^{DsRed} cells preferentially patterned in the center core of the spheroid, as the exterior outside coating of the spheroid, or randomly distributed within the spheroid. Such concentric patterning of spheroids can easily be manipulated using the 384 hanging drop plate by varying the timing and order of seeding the different cell type suspensions into the hanging drops. The ability to access spheroid samples directly from the top of the plate greatly simplifies the multiple pipetting steps required in the 3D patterning. Figure 4c shows time-lapse images of 3D concentric layer patterning of CellTracker Green- and Red-labeled COS7 cells within a spheroid. On Day 1, CellTracker Green-labeled COS7 cells had only aggregated into multiple smaller spheroids that then merged into an irregular-shaped 3D cluster of cells within the hanging drop. By days 2 and 3, cells had re-organized and merged themselves into a more spherical-shaped spheroid. Here, CellTracker Red-labeled COS7 cells were added to the hanging drop already containing a CellTracker Green-labeled COS7 spheroid on Day 3. By Day 4, the red cells started to attach to the outside periphery of the existing green spheroid and subsequently formed into a single spheroid with the green cells. Monoculture of different colored COS7 cells allows for real-time tracking of cellular localizations, migration, and intercellular interactions in 3D. Such technique could be applied to different cell types where valuable biological insights into 3D cellular behavior could be obtained. For example, using a microfluidic device, we have observed HepG2 cells initially randomly mixed with MDA-MB-231 breast cancer cells to self-organize to stay on the outer surfaces of MDA-MB-231 spheroids, similar to the patterned concentric layer spheroids (Torisawa et al., 2009). Likewise, it would also be interesting to observe how two heterotypic cell types initially patterned concentrically self-organize themselves. Such patterning easily enabled by the 384 hanging drop array provide new approaches to understand and manipulate heterotypic cellular interactions in 3D. A special note to consider is that depending on the cell type, it is normal

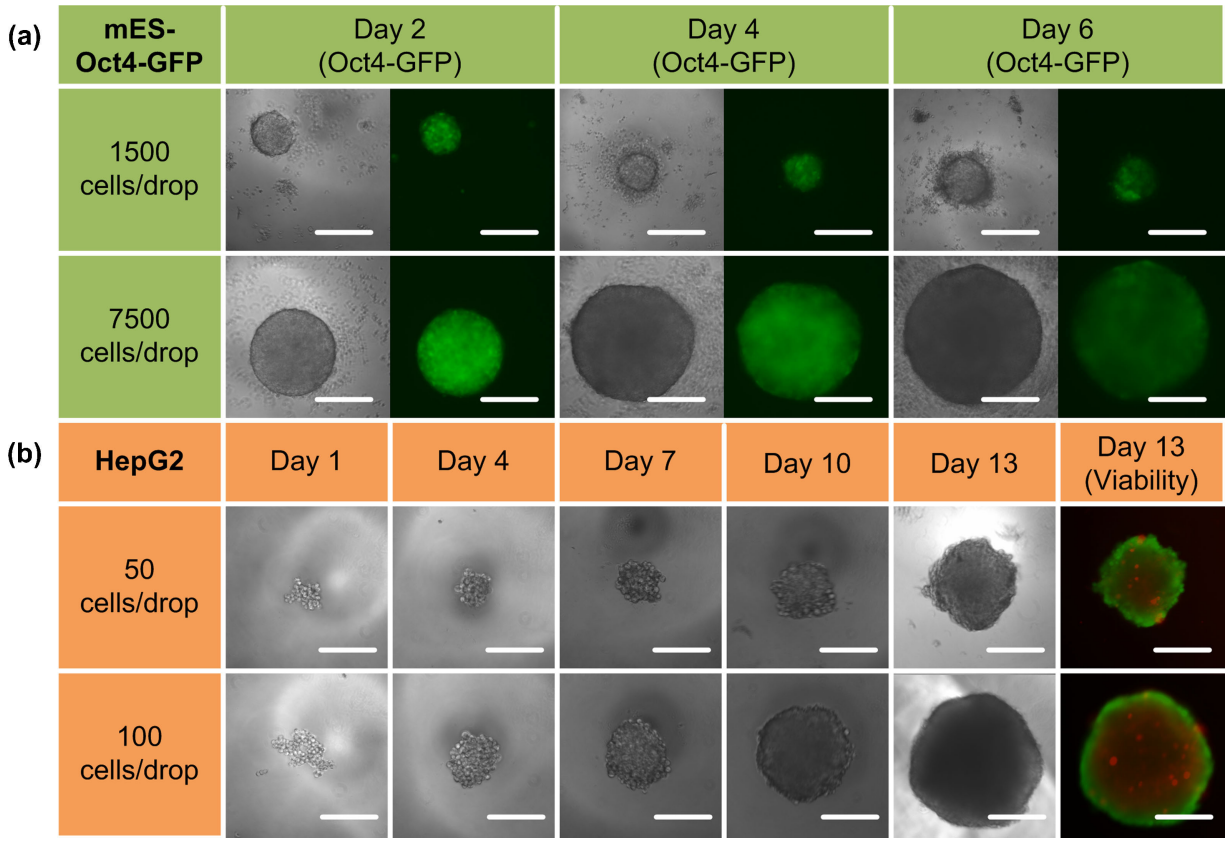

Figure 2. **a**: Time-lapse images of mES-Oct4-GFP cell embryoid bodies cultured in the 384 hanging drop array plate at two initial seeding densities. GFP green fluorescence represents cells that still express Oct4. **b**: Time-lapse images of HepG2 cell spheroids cultured in the 384 hanging drop array plate at two initial seeding densities. On Day 13, a viability staining was performed where green represents live cells and red represents dead cells. All embryoid bodies and spheroids were cultured in 15 μL hanging drops. Scale bar is 200 μm. [Color figure can be seen in the online version of this article, available at http://wileyonlinelibrary.com/bit]

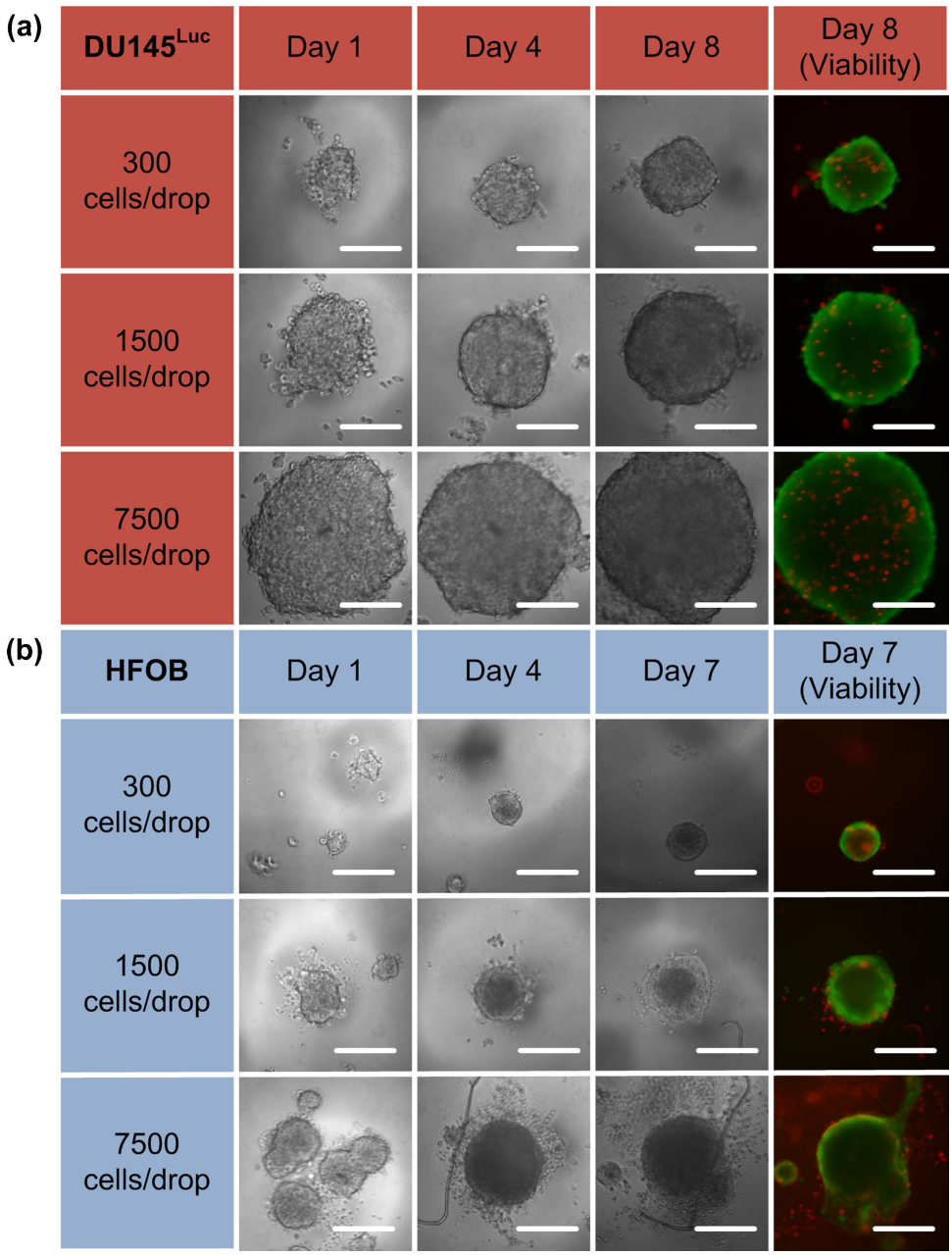

Figure 3. **a**: Time-lapse images of DU145^{Luc} prostate cancer spheroids cultured in the 384 hanging drop array plate at three initial seeding densities. On Day 8, a viability staining was performed where green represents live cells and red represents dead cells. **b**: Time-lapse images of HFOB spheroids cultured in the 384 hanging drop array plate at three initial seeding densities. On Day 7, a viability staining was performed where green represents live cells and red represents dead cells. All spheroids were cultured in 15 μL hanging drops. Scale bar is 200 μm. [Color figure can be seen in the online version of this article, available at http://wileyonlinelibrary.com/bit]

for some cells to form into slightly irregular-shaped 3D cluster of cells or "spheroids" that might not be perfectly spherical in shape. But for most cell types, given enough time, the cells will eventually merge and re-organize into spherical-shaped spheroids as in the case of COS7 cells shown in Figure 4c from days 1 to 3.

Finally, we demonstrate that spheroids cultured in the 384 hanging drop plates can be easily retrieved and transferred to another existing hanging drop (Fig. 5a) to form Janus spheroids. Janus spheroids are spheroids composed of two groups of cells juxtaposed non-concentrically next to each other, so that each group of cells essentially forms a hemisphere. We have previously demonstrated Janus spheroid patterning of HepG2 cells with mES cells and MDA-MB-231 breast cancer cells with COS7 cells using hydrodynamic patterning within a microfluidic device (Torisawa et al., 2009). However, the utility of the microfluidic device is limited by the difficulty involved in

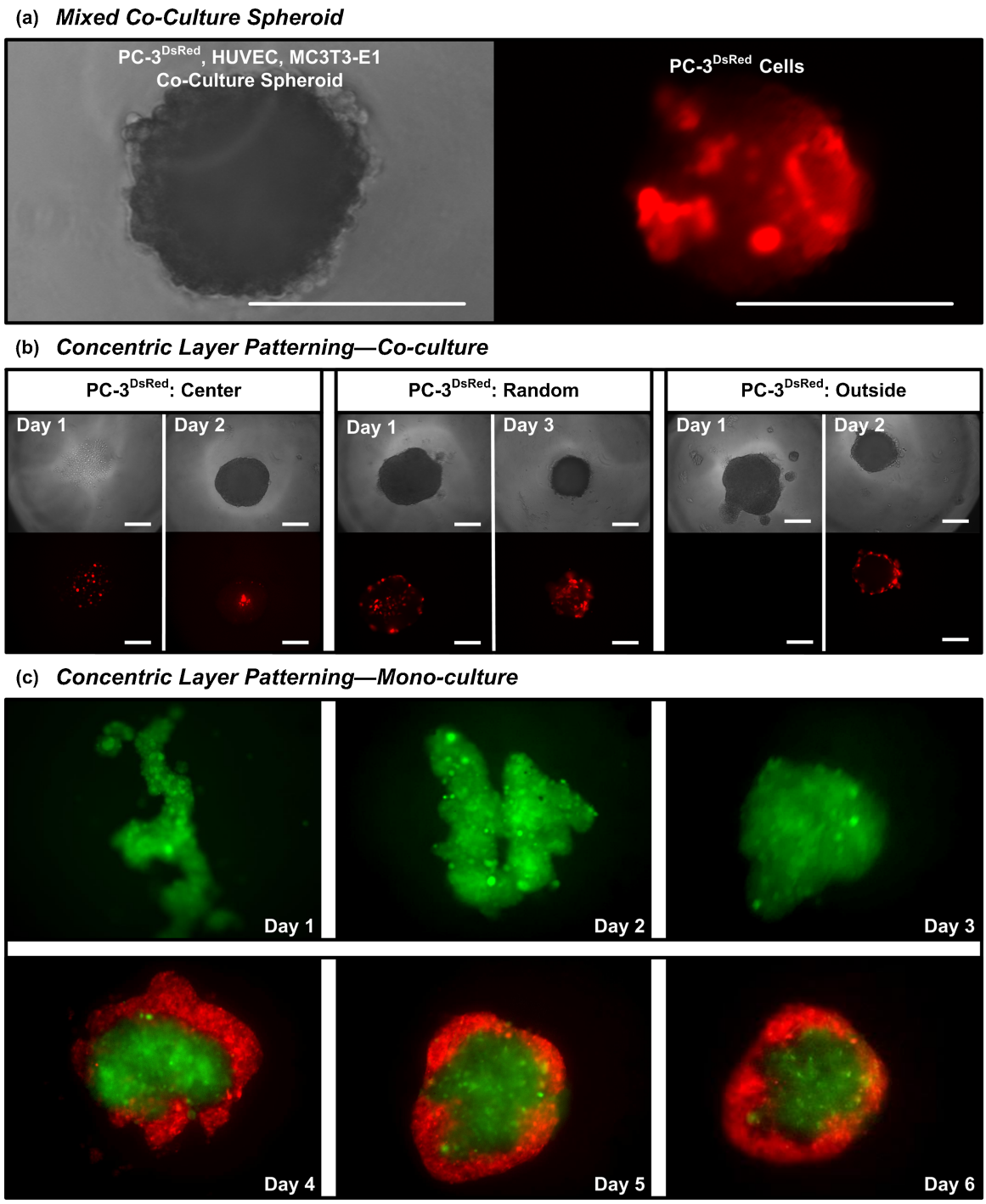

Figure 4. **a**: Phase and fluorescent images of a PC-3^{DsRed}, HUVEC, MC3T3-E1 (1:50:50 ratio) mixed co-culture spheroid. **b**: Images of PC-3^{DsRed} and MC3T3-E1 (1:100 ratio) co-culture spheroids with PC-3^{DsRed} cells preferentially patterned in the center, exterior, or randomly distributed. **c**: Time-lapse images of CellTracker Green- and Red-labeled COS7 cells patterned into concentric layers within a spheroid, where CellTracker Red-labeled COS7 cells were added to the hanging drop on day 3 and thereafter attach to the outside periphery of the existing green spheroid. All spheroids were initially cultured in 15 μL hanging drops. For the concentrically patterned spheroids in (**b**) and (**c**), 5 μL of the second cell suspension was subsequently added to the existing 15 μL droplets, bringing the final total hanging drop volume to 20 μL. Scale bar is 200 μm. [Color figure can be seen in the online version of this article, available at http://wileyonlinelibrary.com/bit]

subsequent spheroid retrieval, short-term culture due to cells eventually attaching to device surfaces, and the complexity involved in device fabrication and operation. Recently, merging of embryoid bodies into Janus spheroids has also been achieved through magnetic manipulation of embryoid bodies incorporated with magnetic microparticles (Bratt-Leal et al., 2011). Such spatial patterning of spheroids was controlled magnetically, which would require spheroid

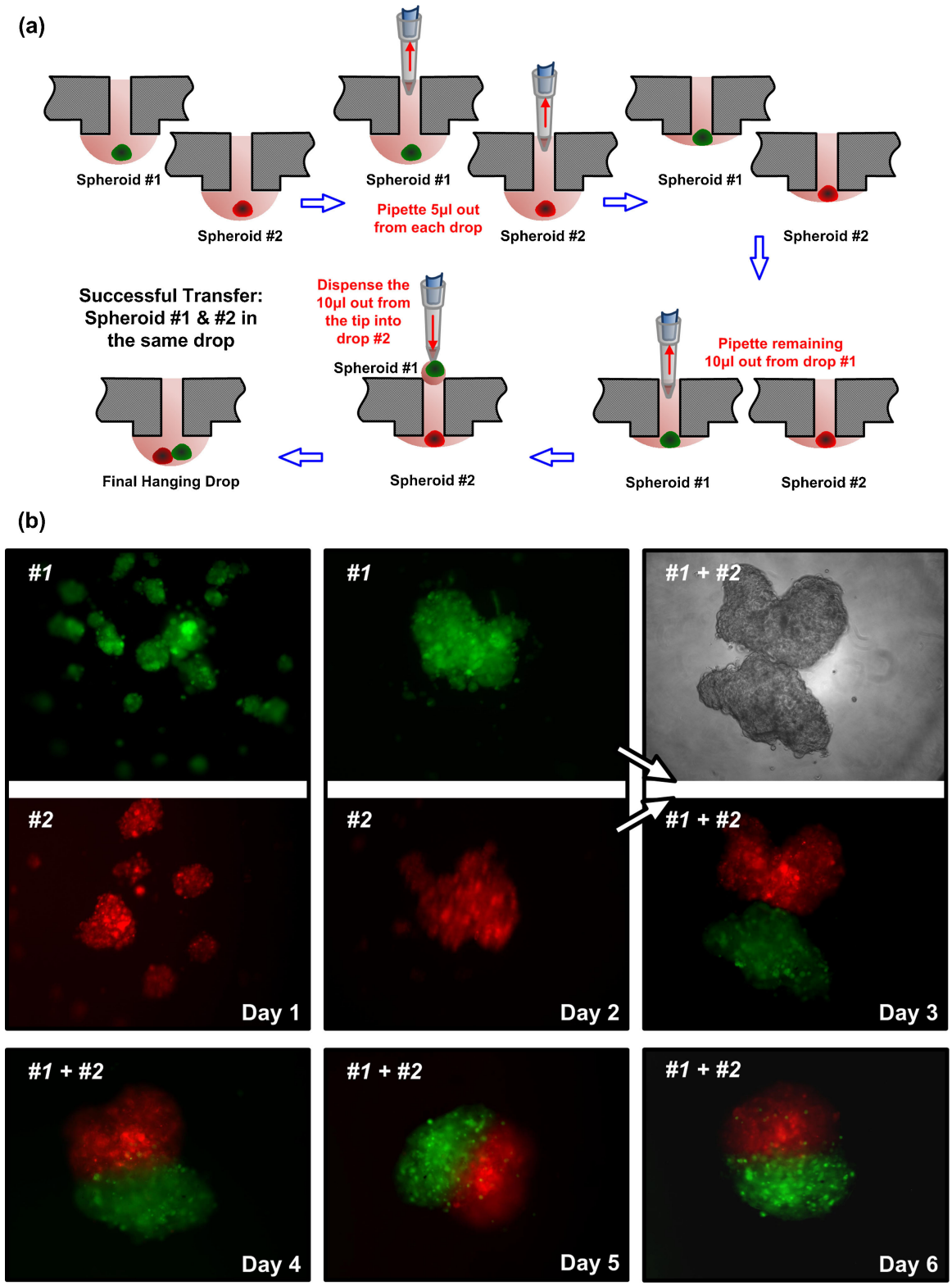

Figure 5. **a**: Cartoon illustrating the process of spheroid transfer between hanging drops in the 384 hanging drop array plate. Initially each spheroid is cultured in a 15 μL hanging drop, and 5 μL of media is removed from each drop. All the remaining 10 μL from drop #1 (including spheroid #1) is subsequently pipetted and transferred to the remaining 10 μL of drop #2. The final drop contains both spheroid #1 and spheroid #2 in 20 μL of media. **b**: Actual time-lapse images of CellTracker Green- and Red-labeled COS7 spheroids before (Days 1 and 2) and after (Days 3, 4, 5, and 6) transfer between hanging drops in the 384 hanging drop array plate. COS7 cells formed into multiple small spheroids per hanging drop on day 1 and subsequently aggregated into single spheroid per drop by Day 2. Upon transferring the green spheroid (#1) into the hanging drop containing the red spheroid (#2), the two spheroids slowly aggregated together over the next 4 days and formed into a single Janus spheroid by Day 6. [Color figure can be seen in the online version of this article, available at http://wileyonlinelibrary.com/bit]

samples to be incorporated with magnetically sensitive microparticles in the first place. The simple user-interface of the 384 hanging drop array plate easily enables researchers to achieve the same Janus spheroid patterning more efficiently. Figure 5b shows the before and after images of a green COS7 spheroid being transferred to a red COS7 spheroid. COS7 cells initially formed into multiple small spheroids per hanging drop on Day 1. Within 1 day, COS7 cells then aggregated into a single spheroid per drop by Day 2. Once each of the red and green cell samples formed into single spheroids, the green spheroid was transferred into the hanging drop containing the red spheroid. Over the next few days, the two spheroids were maintained in such confrontation cultures and slowly aggregated together to form a single Janus spheroid with half green cells and half red cells by Day 6. This process can be easily performed on the hanging drop plate by simple manual pipetting or pipetting by a robotic liquid handler from the top side of the plate. Such a technique is useful in 3D confrontational studies or formation of Janus spheroids (given enough time for the two spheroids to merge) where cell–cell interactions in 3D can be studied. In addition, spheroid transfer allows for 3D side-by-side patterning for tissue engineering purposes as well as differentiation studies of embryoid bodies co-cultured next to a second cell type (Torisawa et al., 2009; Wartenberg et al., 2001). By combining the concentric layer patterning technique with Janus spheroid formation, it could also be possible to reconstruct complicated biomimetic tissue or organ patterns in vitro. Finally, it should be noted that for some heterotypic co-culture of two cell types, Janus spheroid may not be formed due to the intrinsic cellular interaction dynamics of each cell type. In such cases where two different cell types tend to segregate from each other, the transfer of one spheroid to another existing hanging drop containing another spheroid would simply result in side-by-side culture of two spheroids, where interesting paracrine signaling studies could be conducted within each hanging drop compartment.

Conclusion

We describe the characterization, enhancement, and versatility of the 384 hanging drop array plate for HTS and biomedical studies. The 3D spheroid culture platform offers excellent and robust assay performance required by HTS in drug discovery and therapeutic development industries. The 384 hanging drop plate is also compatible with a wide variety of cell types. We further demonstrate simple method to pattern cells three-dimensionally in pre-arranged positions that would otherwise be difficult due to the intrinsic cellular binding characteristics. Special spheroid manipulation techniques enabled by the platform to create different types of co-culture spheroids open up novel ways to study cancer biology, developmental biology, and tissue engineering in 3D. We believe the high-throughput hanging drop platform will be a valuable tool capable of impacting current 3D cell culture standards in a wide range of disciplines.

We thank Dr. Grembecka for kindly providing the PHERAStar FS microplate reader. We also thank Dr. O'Shea for generously providing the mES-Oct4-GFP cell line. This material is based upon work supported by the Coulter Foundation, and the College of Engineering Translational Research Fund. A. Y. H. acknowledges a Horace H. Rackham Predoctoral Fellowship from the University of Michigan. K. J. P. acknowledges NIH 1 PO1 CA093900 for grant support.

References

Baraniak PR, McDevitt TC. 2011. Scaffold-free culture of mesenchymal stem cell spheroids in suspension preserves multilineage potential. Cell Tissue Res. DOI: 10.1007/s00441-011-1215-5.

Birmingham A, Selfors LM, Forster T, Wrobel D, Kennedy CJ, Shanks E, Santoyo-Lopez J, Dunican DJ, Long A, Kelleher D, Smith Q, Beijersbergen RL, Ghazal P, Shamu CE. 2009. Statistical methods for analysis of high-throughput RNA interference screens. Nat Methods 6:569–575.

Bratt-Leal AM, Kepple KL, Carpenedo RL, Cooke MT, McDevitt TC. 2011. Magnetic manipulation and spatial patterning of multi-cellular stem cell aggregates. Integr Biol 3:1224–1232.

Friedrich J, Ebner R, Kunz-Schughart LA. 2007. Experimental anti-tumor therapy in 3-D: Spheroids-old hat or new challenge. Int J Radiat Biol 83:849–871.

Friedrich J, Seidel C, Ebner R, Kunz-Schughart LA. 2009. Spheroid-based drug screen: Considerations and practical approach. Nat Protoc 4:309–324.

Fukuda J, Khademhosseini A, Yeo Y, Yang X, Yeh J, Eng G, Blumling J, Wang CF, Kohane DS, Langer R. 2006. Micromolding of photocrosslinkable chitosan hydrogel for spheroid microarray and co-cultures. Biomaterials 27:5259–5267.

Hirschhaeuser F, Menne H, Dittfeld C, West J, Mueller-Klieser W, Kunz-Schughart LA. 2010. Multicellular tumor spheroids: An underestimated tool is catching up again. J Biotechnol 148:3–15.

Hsiao AY, Torisawa YS, Tung YC, Sud S, Taichman RS, Pienta KJ, Takayama S. 2009. Microfluidic system for formation of PC-3 prostate cancer co-culture spheroids. Biomaterials 30:3020–3027.

Ingram M, Techy GB, Saroufeem R, Yazan O, Narayan KS, Goodwin TJ, Spaulding GF. 1997. Three-dimensional growth patterns of various human tumor cell lines in simulated microgravity of a NASA bioreactor. In Vitro Cell Dev Biol Anim 33:459–466.

Kalikin LM, Schneider A, Thakur MA, Fridman Y, Griffin LB, Dunn RL, Rosol TJ, Shah RB, Rehemtulla A, McCauley LK, Pienta KJ. 2003. In vivo visualization of metastatic prostate cancer and quantitation of disease progression in immunocompromised mice. Cancer Biol Ther 2:656–660.

Karp JM, Yeh J, Eng G, Fukuda J, Blumling J, Suh KY, Cheng J, Mahdavi A, Borenstein J, Langer R, Khademhosseini A. 2007. Controlling size, shape and homogeneity of embryoid bodies using poly(ethylene glycol) microwells. Lab Chip 7:786–794.

Kojima R, Yoshimoto K, Takahashi E, Ichino M, Miyoshi H, Nagasaki Y. 2009. Spheroid array of fetal mouse liver cells constructed on a PEG-gel micropatterned surface: Upregulation of hepatic functions by co-culture with nonparenchymal liver cells. Lab Chip 9:1991–1993.

Lee WG, Ortmann D, Hancock MJ, Bae H, Khademhosseini A. 2010. A hollow sphere soft lithography approach for long-term hanging drop methods. Tissue Eng Part C Methods 16:249–259.

Lin RZ, Chang HY. 2008. Recent advances in three-dimensional multicellular spheroid culture for biomedical research. Biotechnol J 3:1172–1184.

Powers MJ, Domansky K, Kaazempur-Mofrad MR, Kalezi A, Capitano A, Upadhyaya A, Kurzawski P, Wack KE, Stolz DB, Kamm R, Griffith LG. 2002. A microfabricated array bioreactor for perfused 3D liver culture. Biotechnol Bioeng 78:257–269.

Qu X. 2011. Design and analysis of high-throughput screening experiments. J Syst Sci Complex 24:711–724.
Sakai Y, Nakazawa K. 2007. Technique for the control of spheroid diameter using microfabricated chips. Acta Biomater 3:1033–1040.
Shields K, Ackland ML, Ahmed N, Rice GE. 2009. Multicellular spheroids in ovarian cancer metastases: Biology and pathology. Gynecol Oncol 113:143–148.
Sui Y, Wu Z. 2007. Alternative statistical parameter for high-throughput screening assay quality assessment. J Biomol Screen 12:229–234.
Tamura T, Sakai Y, Nakazawa K. 2008. Two-dimensional microarray of HepG2 spheroids using collagen/polyethylene glycol micropatterned chip. J Mater Sci Mater Med 19:2071–2077.
Toh YC, Zhang C, Zhang J, Khong YM, Chang S, Samper VD, van Noort D, Hutmacher DW, Yu H. 2007. A novel 3D mammalian cell perfusion-culture system in microfluidic channels. Lab Chip 7:302–309.
Toh YC, Lim TC, Tai D, Xiao G, van Noort D, Yu H. 2009. A microfluidic 3D hepatocyte chip for drug toxicity testing. Lab Chip 9:2026–2035.
Torisawa YS, Chueh BH, Huh D, Ramamurthy P, Roth TM, Barald KF, Takayama S. 2007a. Efficient synchronous formation of uniform-sized embryoid bodies using a compartmentalized microchannel device. Lab Chip 7:770–776.
Torisawa YS, Takagi A, Nahimoto Y, Yasukawa T, Shiku H, Matsue T. 2007b. A multicellular spheroid array to realize spheroid formation, culture, and viability assay on a chip. Biomaterials 28:559–566.
Torisawa YS, Mosadegh B, Luker GD, Morell M, O'Shea KS, Takayama S. 2009. Microfluidic hydrodynamic cellular patterning for systematic formation of co-culture spheroids. Integr Biol 1:649–654.
Tung YC, Hsiao AY, Allen SG, Torisawa YS, Ho M, Takayama S. 2011. High-throughput 3D spheroid culture and drug testing using a 384 hanging drop array. Analyst 136:473–478.
Ungrin MD, Joshi C, Nica A, Bauwens C, Zandstra PW. 2008. Reproducible, ultra high-throughput formation of multicellular organization from single cell suspension-derived human embryonic stem cell aggregates. PLoS ONE 3:e1565.
Wartenberg M, Donmez F, Ling FC, Acker H, Hescheler J, Sauer H. 2001. Tumor-induced angiogenesis studied in confrontation cultures of multicellular tumor spheroids and embryoid bodies grown from pluripotent embryonic stem cells. FASEB J 15:995–1005.
Wu LY, DiCarlo D, Lee LP. 2008. Microfluidic self-assembly of tumor spheroids for anticancer drug discovery. Biomed Microdev 10:197–202.
Yamada KM, Cukierman E. 2007. Modeling tissue morphogenesis and cancer in 3D. Cell 130:601–610.
Yoshii Y, Waki A, Yoshida K, Kakezuka A, Kobayashi M, Namiki H, Kuroda Y, Kiyono Y, Yoshii H, Furukawa T, Asai T, Okazawa H, Gelovani JG, Fujibayashi Y. 2011. The use of nanoimprinted scaffolds as 3D culture models to facilitate spontaneous tumor cell migration and well-regulated spheroid formation. Biomaterials 32:6052–6058.
Zhang JH, Chung TD, Oldenburg KR. 1999. A simple statistical parameter for use in evaluation and validation of high throughput screening assays. J Biomol Screen 4:67–73.
Zhang MY, Lee PJ, Hung PJ, Johnson T, Lee LP, Mofrad MR. 2008. Microfluidic environment for high density hepatocyte culture. Biomed Microdev 10:117–121.